

# Ultrafast-Laser-Absorption-Spectroscopy Measurements of Temperature and CO in High-Pressure, Multi-Phase Propellant Flames

Ryan J. Tancin \* Morgan D. Ruesch † Steven F. Son ‡ Robert P. Lucht § Christopher S. Goldenstein ¶ Purdue University, West Lafayette, IN, 47907, United States

This manuscript describes the first application of ultrafast-laser-absorption spectroscopy (ULAS) to characterizing high-pressure (up to 40 bar), multi-phase combustion gases. Singleshot measurements of temperature and CO were acquired at 5 kHz in AP-HTPB propellant flames with and without aluminum. An ultrafast light source was used to produce broadband pulses of light near 4.96  $\mu$ m at a repetition rate of 5 kHz and a high-speed mid-infrared imaging spectrometer was used to image the pulses across an 86 nm bandwidth with a spectral resolution of 0.7 nm. Measurements of temperature and CO concentration were obtained by least-squares fitting simulated absorbance spectra of CO to measured spectra. A system of corrective optics was used to diminish the effect of beam steering during high-pressure experiments, greatly increasing the pressure capabilities of the diagnostic. The diagnostic was used to characterize AP-HTPB propellant flames in an argon bath gas at pressures of 1, 10, 20, and 40 bar. An aluminized AP-HTPB propellant was also characterized at 10 and 20 bar to demonstrate that ULAS can provide high-fidelity measurements in particulate-laden flames. The results demonstrate that ULAS is capable of providing single-shot temperature and species measurements at high pressures with 1- $\sigma$  precisions less than 1.1% and 3% for temperature and species respectively, despite non-absorbing transmission losses in excess of 90%.

# I. Nomenclature

incident (baseline) laser intensity (a.u.)  $I_0$ transmitted laser intensity (a.u.)  $I_t$ Labsorbing path length (cm) collisional-broadening temperature exponent nTtemperature (K) measured spectral absorbance  $\alpha(\nu)_{measured}$ perturber-specific collisional-broadening coefficient (cm<sup>-1</sup>/atm)  $\gamma$ optical frequency (cm<sup>-1</sup>) ν collisional full-width at half-maximum (cm<sup>-1</sup>)  $\nu_c$ absorbing species mole fraction Xabs

#### II. Introduction

There remains a general need for non-invasive diagnostics capable of measuring gas properties in harsh, high-pressure environments representative of those encountered in practical combustors [1, 2]. Acquiring laser-absorption-spectroscopy (LAS) measurements in such environments, particularly those at elevated pressures, imposes a number of

<sup>\*</sup>Graduate Research Assistant, School of Aeronautics and Astronautics, 701 W Stadium Ave, West Lafayette, IN 47907, and AIAA Student Member

<sup>&</sup>lt;sup>†</sup>Graduate Research Assistant, School of Aeronautics and Astronautics, 701 W Stadium Ave, West Lafayette, IN 47907, and AIAA Student Member

<sup>&</sup>lt;sup>‡</sup>Alfred J. McAllister Professor, School of Mechanical Engineering, 585 Purdue Mall, West Lafayette, IN 47907, AIAA Associate Fellow <sup>§</sup>Ralph and Bettye Bailey Distinguished Professor of Mechanical Engineering, School of Mechanical Engineering, 585 Purdue Mall, West Lafayette, IN 47907, AIAA Fellow

<sup>¶</sup>Assistant Professor, School of Mechanical Engineering, 585 Purdue Mall, West Lafayette, IN 47907, AIAA Senior Member

challenges. For example, spectroscopic challenges arise from increased collisional broadening, which can complicate determination of gas properties by, for example, blending lines, reducing levels of differential absorption, and increasing uncertainty in the non-absorbing baseline due to the absence of non-resonant wavelengths [1]. Frequently, the greatest challenge in acquiring LAS measurements in harsh environments is tolerating non-absorbing transmission losses arising from beam steering, window fouling, and scattering and attenuation by particulates and droplets. In addition, pressure-induced reduction of combustion-relevant length- and time-scales can present further difficulties.

Non-absorbing transmission losses can reduce the accuracy and precision of LAS measurements primarily because they complicate the accurate determination of the baseline laser intensity [3, 4] and, secondarily, because they reduce the measurement signal-to-noise ratio (SNR). These challenges can be mitigated through: (1) using wavelength-modulation spectroscopy (WMS) [5–8] or emerging free-induction-decay-based data-processing techniques [3, 4] to avoid the need to accurately model the baseline laser intensity, (2) using a broadband light source which facilitates *in situ* determination of the baseline light intensity by collecting more diverse spectral information [9–12], or (3) acquiring measurements rapidly such that non-absorbing losses are "frozen" on the time scale of the measurement, which avoids the need for more complex baseline-correction strategies [9, 13, 14]. LAS diagnostics which are successful at making measurements in harsh, high-pressure environments typically employ one or more of these strategies [1].

Diagnostics employing baseline-insensitive or, arguably, baseline-free techniques, most notably WMS-2f/1f, have demonstrated the ability to measure gas properties in a variety of harsh, high-pressure combustion environments such as rocket engines [5], rotating-detonation engines (RDEs) [8] and pulse-detonation combustors (PDCs) [7]. For example, three tunable-diode lasers (TDLs) and one quantum-cascade laser (QCL) were used with WMS-2f/1f to measure  $H_2O$  (near 1.4 and 2.5  $\mu$ m), CO (near 4.85  $\mu$ m), CO<sub>2</sub> (near 2.7  $\mu$ m), and temperature in an ethlyene-fueled PDC [7]. Measurements were collected at rates between 2 and 20 kHz at pressures ranging from 1 to 50 atm (for T, CO and  $H_2O$ ) and 1 to 12 atm (for  $CO_2$ ). More recently, Bendana et al. [5] used scanned-WMS-2f/1f to measure temperature and CO within a kerosene-fueled rocket combustor at pressures ranging from 25 to 80 bar, and measurements of CO were acquired up to 106 bar. Measurements were acquired using a TDL near 2.3  $\mu$ m and a QCL near 4.98  $\mu$ m.

Diagnostics which exploit broad spectral bandwidth to help overcome non-absorbing transmission losses have utilized both wavelength-tunable lasers with large tuning ranges (e.g., vertical-cavity surface-emitting lasers (VCSELs)) and broadband pulsed light sources (e.g., ultrafast lasers, frequency combs). For example, Sanders et al. [15] used a VCSEL to make measurements of temperature and atomic cesium in a cesium-seeded PDC. The laser was scanned across a  $10 \text{ cm}^{-1}$  spectral window which enabled measurements to be acquired at pressures as high as 33 atm. Time-division-multiplexed (TDM) Fourier-domain mode-locked (FDML) lasers were utilized by Caswell et al. [10] to acquire measurements of  $H_2O$ , temperature, pressure and velocity in an  $H_2$ -air fueled PDC. Measurements were acquired near  $1.35 \mu m$  with greater than  $15 \text{ cm}^{-1}$  of bandwidth. Most recently, dual frequency-comb spectrometers which rely on a pulsed femtosecond lightsource have been used to acquire broadband absorption measurements. For example, Draper et al. [12] used a dual frequency-comb spectrometer with  $160 \text{ cm}^{-1}$  of bandwidth to make measurements of  $CH_4$  and temperature near  $6086 \text{ cm}^{-1}$  inside of a rapid compression machine at pressures up to 30 bar.

Lastly, numerous direct absorption and WMS techniques have relied on acquiring measurements rapidly to effectively "freeze" non-absorbing transmission losses on the the time scale of the measurement. For example, a MEMS VCSEL capable of scanning from 1330 to 1365 nm at 100 kHz has been utilized by Rein et al. [14] to acquire high-speed measurements of temperature and  $H_2O$  within the annulus of an  $H_2$ -air RDE. In addition, Nair et al. [13] performed rapid wavelength scanning of a distributed feedback (DFB) QCL and an interband-cascade laser (ICL) at 5  $\mu$ m and 4.19  $\mu$ m, respectively, to measure temperature, pressure, CO and CO<sub>2</sub> at 1 to 3 MHz at the exit of a CH<sub>4</sub>-O<sub>2</sub> fueled RDE. Soon after, Mathews et al. [16] utilized a similar QCL-based diagnostic to measure temperature, pressure, and CO at 750 kHz and a pair of TDLs emitting near 1.4  $\mu$ m to measure temperature and  $H_2O$  at 1 MHz in the annulus of the same CH<sub>4</sub>-O<sub>2</sub> fueled RDE. The TDLAS diagnostic relied on near-GHz scanned-WMS-2 f/1f to improve measurement SNR and achieve measurements at 1 MHz [17].

Recently, we have developed an ultrafast-laser-absorption-spectroscopy (ULAS) diagnostic [9] to provide multiparameter measurements of gas temperature and species (CO, NO, CO<sub>2</sub>, H<sub>2</sub>O, CH<sub>4</sub>) with sub-nanosecond time resolution [9, 18, 19]. ULAS possesses a number of attributes which make it well suited for characterizing harsh combustion environments. First, it can provide single-shot measurements with sub-nanosecond time resolution [9, 18], which is typically limited by the pulse's time of flight through the test gas. Secondly, it provides broad-bandwidth measurements which facilitates high-dynamic-range thermometry and *in situ* determination of the baseline light intensity despite the absence of non-resonant wavelengths. In this work, we demonstrate that these attributes enable ULAS to tolerate pronounced non-absorbing transmission losses encountered in high-pressure, multi-phase propellant flames. More specifically, we demonstrate this through measurements of temperature and  $\chi_{CO}$  acquired in ammonium perchlorate (AP), hydroxyl-terminated polybutadiene (HTPB) propellant flames, both with and without aluminum, at pressures up to 40 bar.

# III. Experimental Details

#### A. Wavelength Selection

Measurements of temperature and CO concentration were acquired using wavelengths from approximately 4914 nm  $(2035 \text{ cm}^{-1})$  to 5000 nm  $(2000 \text{ cm}^{-1})$ . This spectral window provides access to high-energy transitions in the P-branch of CO's fundamental vibration bands. This window was chosen for three primary reasons: (1) spectral interference from  $H_2O$ ,  $CO_2$ , and NO is weak at the conditions of interest, (2) it provides near optimal absorbance levels at equilibrium conditions in lab-scale AP-HTPB flames, and (3) it provides excellent temperature sensitivity due to the presence of high-rotational-energy transitions within numerous vibrational levels [18, 20].

# **B.** Optical Setup

A schematic of the optical setup is shown in Fig. 1. The laser system used in this work utilized a Ti:Sapphire oscillator (Coherent Mantis) which produced ultrashort pulses of light at a repetition rate of 80 MHz. The pulses were centered near 800 nm with an initial pulse duration of approximately 55 fs. The laser pulses were passed to a pulse shaper (FemtoJock) where they were tailored for amplification by a regenerative, multi-stage amplifier (Coherent Legend Elite Duo). The amplifier selectively amplified the pulses to an energy of 2 mJ/pulse at a repetition rate of 5 kHz. Additional amplification and conversion into the mid-IR was achieved through optical parametric amplification (OPA) and non-collinear difference-frequency generation (NDFG) processes inside a Coherent OPerA Solo module. Ultrashort

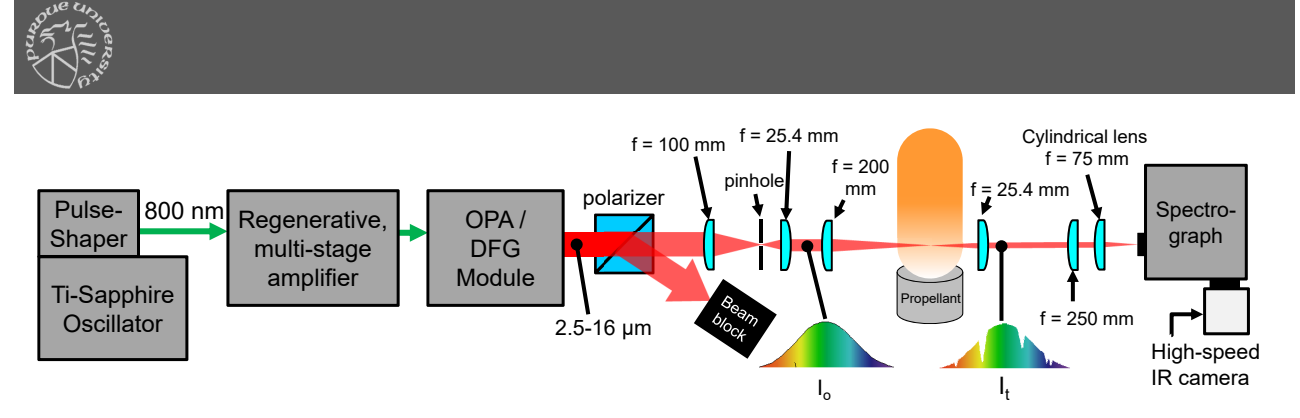


Fig. 1 Schematic illustrating the optical setup used to characterize propellant flames with ULAS.

A MgF<sub>2</sub> Rochon-prism polarizer was used to attenuate the laser beam through adjusting the rotational position of the polarizer. Next, a spatial filter was used for the purpose of improving the spatial profile of the laser beam and reducing the beam diameter. The spatial filter consisted of an anti-reflection (AR) coated, CaF<sub>2</sub>, plano-convex lens with a 100 mm focal length which focused the laser-beam through a 100  $\mu$ m pinhole. The beam was then re-collimated using an AR coated, Si, plano-convex lens with a 25.4 mm focal length. The  $1/e^2$  beam diameter immediately downstream of the spatial filter was approximately 2 mm.

The laser beam was directed through the test gas within either a static-gas cell or propellant flame. Corrective optics (discussed at length in Sect. III.C) were applied here to reduce the impact of beam steering on flame measurements which was particularly important due to the long ( $\approx 1$  m) path length from the flame to the spectrometer. The transmitted pulses were then focused onto the input slit of an imaging spectrometer (Andor Shamrock 500i) using a CaF<sub>2</sub>, plano-convex, cylindrical lens with a focal length of 75 mm. The imaging spectrometer employed a reflective diffraction grating to disperse the light onto the InSb focal plane array of a high-speed, infrared camera (Telops FAST-IR 2K). In this configuration, the IR camera recorded spectral information in the x-dimension and 1D spatial information in the y-dimension. In propellant tests, single-shot spectra were averaged across the spatial dimension to improve the measurement SNR. Two diffraction gratings were used: (1) A comparatively low-resolution grating with 150 lines/mm

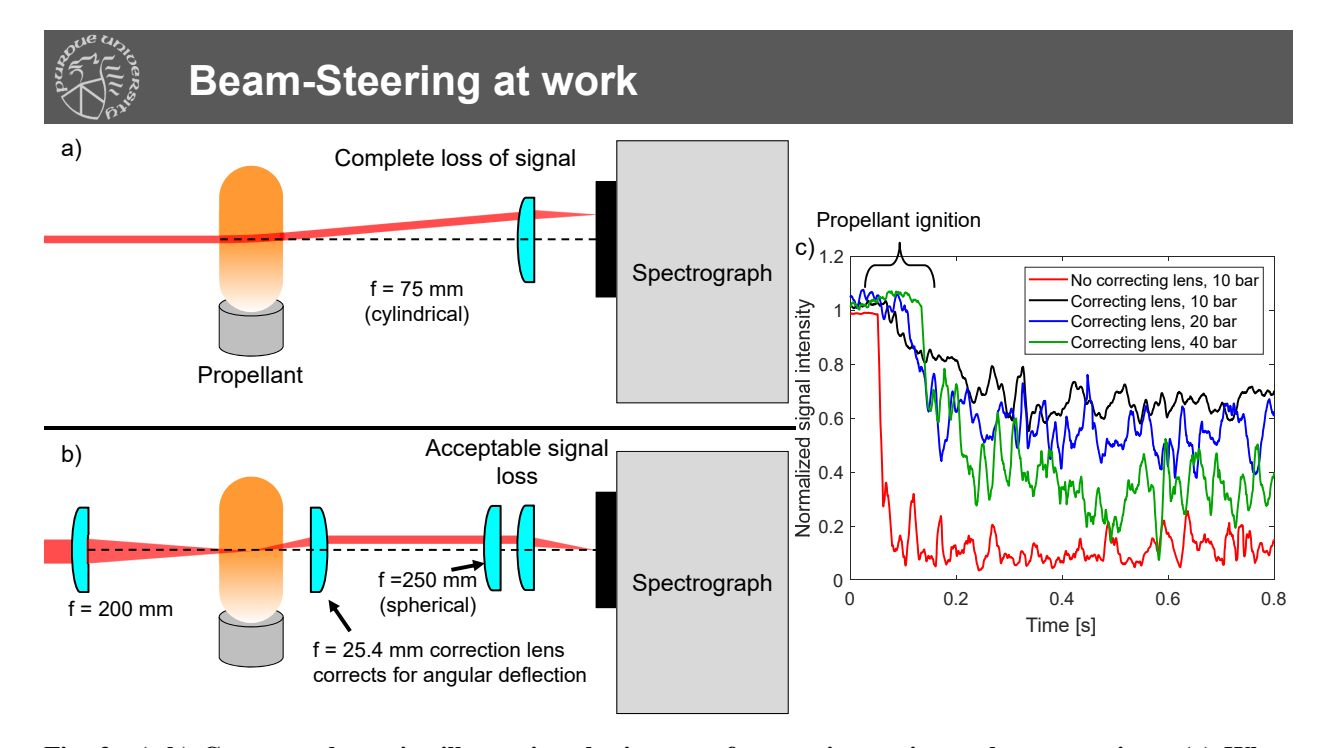


Fig. 2 (a,b) Concept schematics illustrating the impact of correcting optics on beam steering. (a) When no correcting optics are used, beam steering leads to a large translational offset in the beam location at the measurement location, resulting in total signal loss. (b) When correcting optics are used, the translational offset in beam location at the measurement location is smaller which leads to a tolerable reduction in signal intensity. (c) Normalized, spectrally averaged light intensity as a function of time in propellant tests at various pressures with and without correcting optics. Using correcting optics significantly reduces transmission losses.

was used to characterize high-pressure gases and (2) a high-resolution grating with 300 lines/mm was used to characterize gases at atmospheric pressure. The spectral bandwidth and resolution were  $\approx 35 \text{ cm}^{-1}$  and 0.6 nm, respectively, for the low-resolution grating, and 10 cm<sup>-1</sup> and 0.3 nm, respectively, for the high-resolution grating.

## C. Mitigation of Beam Steering

Beam steering, refers to angular deflections of the laser beam which result from a non-uniform refractive index. In combustion gases, this results from the laser beam passing through density gradients, typically resulting from temperature varying along the beam path. Beam steering often becomes more pronounced at higher pressures due to the steeper density gradients present. Beam steering is most problematic when the distance between the steering medium and the detector is large, as is the case here. In this case a small angular deflection leads to a large translational displacement in the beam location at the detector location, as is illustrated in Fig. 2a. While ULAS can tolerate some non-absorbing transmission losses due to its short measurement time and broad bandwidth, severe beam steering can prevent high-SNR measurements by preventing a sufficient number of photons from being collected. In severe cases, a deflected laser beam may be entirely blocked by an aperture (e.g., the input slit of the spectrometer), thereby precluding measurements.

A lens telescope was employed as shown in Fig. 1 and Fig. 2b in order to reduce the impact of beam steering. The upstream and downstream lenses were a 200 mm focal length, CaF<sub>2</sub>, plano-convex lens and a 25.4 mm focal length, AR-coated, Si, plano-convex lens, respectively. Additionally, a 250 mm focal length, AR-coated, CaF<sub>2</sub> lens was placed directly before the final 75 mm cylindrical lens. By placing the focal point of the lens telescope within the steering medium (i.e., the flame), the re-collimating lens acts to partially correct angular deflections. In this simplified picture, the steered laser beam travels on a path parallel to the original beam path (after passing through the correction lens), albeit with a small offset, which leads to a tolerable transmission loss. These concepts are illustrated in Fig. 2b. The smaller the focal length of the collimating lens, the smaller the offset for a given angular deflection. However, short focal-length lenses are more sensitive to beam steering which originates outside the focal point of the lens. Figure 2c shows the effect of beam steering on the spectrally averaged transmitted light intensity recorded by the IR camera in tests at various pressures with and without the correcting optics used to mitigate beam steering. The results show that when corrective optics were used, the average light intensity recorded by the IR camera increased by a factor of 6. The



Fig. 3 DSLR images of laser-ignited AP-HTPB propellant flames, both without (left four panels) and with (right two panels) aluminum. Images were taken with identical exposure settings (except for the test at 1 bar) to allow for comparison of flame luminosity at different conditions.

lens telescope component of the corrective optics was only used for flame experiments, whereas the 250 mm focal length lens was used for both flame and gas-cell measurements.

## **D. Gas-Cell Experiments**

The accuracy of the ULAS diagnostic was validated by acquiring measurements at known thermodynamic conditions within a heated static-gas cell which is described in detail by Schwarm et al. [21]. The gas cell was heated to  $\approx 1000~\text{K}$  and then filled with a mixture of 2.0% CO and 1.8% CO<sub>2</sub> with a balance of N<sub>2</sub>. Measurements of temperature and CO concentration were acquired at 10, 20 and 40 bar. The gas pressure was measured using a Unik-5000 pressure transducer with a full-scale range of 0 to 70 bar and an accuracy of  $\pm 0.028~\text{bar}$ . Temperature was measured using three type-K thermocouples with a nominal accuracy of 0.75% (at  $\pm 600~\text{K}$ ) fixed to the outside of the gas cell in a configuration identical to that described in [21]. The gas cell was equipped with 15 cm long, wedged, CaF<sub>2</sub> rods, which provided a path length through the test gas of 9.4 cm at room temperature. At 1000 K, the path length of the gas cell is 9.2 cm (2% shorter) due to disparate thermal expansion of the gas cell and CaF<sub>2</sub> rods. The lens telescope portion of the corrective optics described in Sect. III.C was not used for the validation measurements, since the geometry of the gas cell and tube furnace precluded this. However, the 250 mm focal length lens was used for consistency with the setup used for propellant tests.

#### E. Propellant Tests

The ULAS diagnostic was used to characterize AP-HTPB propellant flames both with and without aluminum. The particle size of AP was distributed bimodally with mean diameters of 200  $\mu$ m and 20  $\mu$ m in a coarse-to-fine ratio of 4:1. On a mass basis, the binder consisted of 76.33% HTPB with 15.05% isodecyl pelargonate as the plasticizer, and 8.62% modified MDI isocyanate as the curative. In cases where aluminum was added, Valimet H-30 aluminum with a mean particle diameter of 31  $\mu$ m was used. The AP-HTPB propellant consisted of 80% AP by mass, whereas the AP-HTPB-Al propellant was 68% AP, 15% aluminum and 17% binder by mass. The propellant was cast into plastic tubes and cured for a minimum of 3 days at room temperature. Tests were performed using 4 to 6 mm tall propellant strands with a 7 mm diameter.

The strands were ignited using a  $CO_2$  laser emitting near 10.6  $\mu$ m. The laser delivered an optical intensity of 38 W/cm<sup>2</sup> to the surface of the strand. The data acquisition system was triggered 100 ms prior to the  $CO_2$  laser turning on, to allow for  $I_0$  to be recorded. The  $CO_2$  laser was turned on for 200 ms (400 ms was used at 1 bar) to ignite the strand. Video of each test was recorded with the DSLR camera, to ensure that ignition and burning of each strand was

uniform, and to provide an estimate of the absorbing path-length. The propellant flames reached a quasi-steady state approximately 100 ms after ignition. Figure 3 shows images of the propellant flames acquired using a Nikon D3200 DSLR camera. With the exception of the 1 bar case, each image was taken with identical exposure settings (1/4000 s shutter speed, ISO 200 and F22 f-stop) to allow for direct comparison between different conditions. At 1 bar, the propellant flames were less luminous so the following camera settings were used to maintain proper exposure: 1/200 s shutter speed, ISO 800 and F22 f-stop.

All propellant tests were conducted using a high-pressure combustion chamber, the design of which is described in detail by Tancin et al. [6]. Optical access for the ULAS diagnostic and DSLR camera was provided by a pair of slot-shaped sapphire windows with a clear aperture of 10 cm x 4 cm in the vertical and horizontal dimensions, respectively. The CO2 laser beam was directed into the vessel through a ZnSe window at the top of the chamber. The propellant was placed on a small vertical-translation stage located in the center of the chamber so that the measurement location relative to the strand surface could be accurately controlled. All measurements were acquired through the center-line of the flame at a vertical location of 2 mm above the initial surface location for the AP-HTPB propellant and 1 cm above the initial surface location for the aluminized propellant. Prior to each test, the chamber was evacuated using a vacuum roughing pump before being pressurized with an argon bath gas. The pressure during each test was measured using the same Unik-5000 pressure transducer as was used for the static-gas cell measurements. A time history of pressure was recorded during each test so that a linear regression could be fitted to each pressure trace allowing for the data processing routine to use an updated pressure for each subsequent laser shot. The gas pressure increased by  $\approx 0.6$  bar during each test.

# **IV. ULAS Data Processing**

Single-shot ULAS measurements of transmission spectra were processed using the methods and spectral-fitting routine described previously by Tancin et al. [9, 18]. As a result, in the interest of brevity only the most pertinent details and those which differ from our prior work will be discussed here.

The measured spectral absorbance  $(\alpha(v)_{measured})$  was obtained from single-shot measurements of  $I_t$  and a time-averaged measurement of  $I_0$  using Beer's law. Gas properties were then determined from the measured spectra by least-squares fitting simulated absorbance spectra to measured spectra using a nonlinear least-squares fitting routine employing the Levenberg–Marquardt algorithm. The fitting routine used the following free parameters: (1) gas properties  $(T \text{ and } \chi_{CO})$ , (2) a first-order baseline correction which accounted for shot-to-shot fluctuations in the laser intensity and broadband transmission losses, (3) the frequency of several prominent spectral features (to match the measured and simulated frequency axes), and (4) variables describing the instrument response function (IRF). The IRF was modeled as the weighted sum of a Gaussian and Lorentzian lineshape, and the FWHM and weight (i.e. the balance between Lorentzian and Gaussian components) were both free parameters in the nonlinear fitting routine. In addition, it should be noted that a small spectral window ( $\approx 2.5 \text{ cm}^{-1}$  wide) near 2017 cm<sup>-1</sup> was ignored by the least-squares fitting routine due to the fact that pronounced absorption by atmospheric water precluded high-SNR measurements in this window.

Absorbance spectra of CO and H<sub>2</sub>O (to account for weak interference) were simulated using the methods described by Goldenstein et al. [22]. The HITEMP2019 spectroscopic database [23] was used to simulate absorbance spectra of CO and the HITEMP2010 database [24] was used to simulate absorbance spectra of H<sub>2</sub>O. The collisional FWHM of each transition was modeled assuming each transition was broadened by CO, CO<sub>2</sub>, H<sub>2</sub>O, N<sub>2</sub> and then a single pseudo-species representing all of the remaining bath-gas species. Self-broadening by CO was modeled using the parameters (γ and n) provided by the HITEMP2019 database. The parameters describing CO<sub>2</sub>-, N<sub>2</sub>- and H<sub>2</sub>O-broadening of CO were taken from Hartmann et al. [25]. Collisional-broadening by the remaining species in the flame bath gas was modeled using the parameters provided for air broadening. This approximation is justified for CO since the majority of the remaining bath-gas species are diatomics which are not expected to posses radically different broadening coefficients [13]. Calculations of collisional FWHM were performed assuming that the mole fractions of CO<sub>2</sub>, N<sub>2</sub> and H<sub>2</sub>O were equal to those predicted by HP equilibrium calculations performed using NASA Chemical Equilibrium and Applications (NASA-CEA).

# V. Results and Discussion

#### A. Validation Experiments

Figure 4 shows how the accuracy of the temperature and  $\chi_{CO}$  measurements acquired in the static-gas cell at 1000 K varies with pressure from 10 to 40 bar. All of the temperature measurements fell within 0.75% of the known value, which is the manufacturer-quoted accuracy for the type-K thermocouples that were used to determine the actual gas temperature. In addition, all of the mole-fraction measurements fell within 3% of the known value provided by the supplier of the gas mixture (Airgas). The 1- $\sigma$  precision for the temperature measurements at 10, 20, and 40 bar were 0.1%, 0.1% and 0.18% of the measured values, respectively. Similarly, the 1- $\sigma$  precisions for  $\chi_{CO}$  were 0.3%, 0.2% and 0.5% of the measured value for 10, 20, and 40 bar, respectively. These results demonstrate that ULAS is capable of providing high-fidelity measurements of gas temperature and  $\chi_{CO}$  at pressures which are relevant to practical propulsion systems.

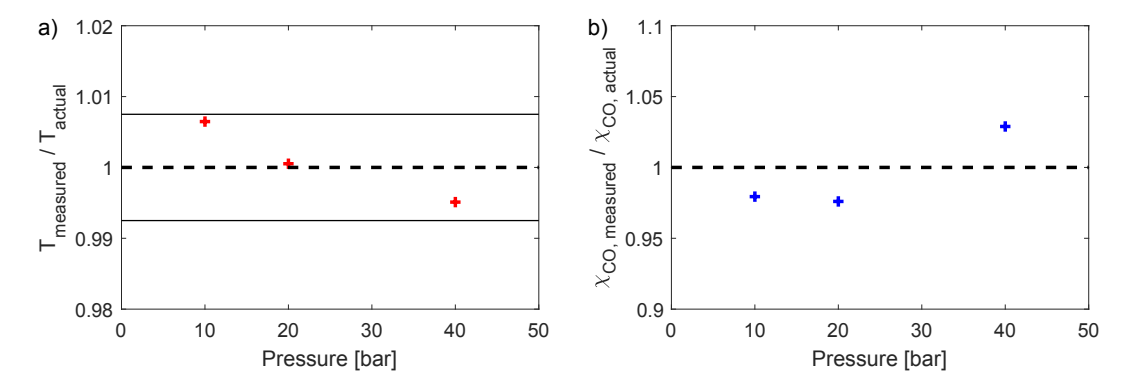


Fig. 4 Accuracy of the ULAS measurements of temperature (a) and  $\chi_{CO}$  (b) acquired in the static-gas cell at 1000 K and pressures of 10, 20, and 40 bar. Measurements are normalized by the known value, hence, the dashed lines represent "perfect" accuracy. The two solid lines represent the uncertainty bounds of the type-K thermocouples used to determine the known gas temperature.

#### B. Characterization of AP-HTPB Propellant Flames

This section presents results acquired in laser-ignited AP-HTPB flames both with and without aluminum. Figure 5 shows measured time histories of T and  $\chi_{CO}$  as well as representative examples of measured and best-fit spectra. The spectra illustrate the high SNR of the measurements and, for all data sets, significant wavelength-dependent structure was not observed in the residuals between measured and best-fit spectra, thereby supporting the accuracy of the spectroscopic model employed. The 1- $\sigma$  precision of the baseline noise level in absorbance was 0.01, 0.005 and 0.006 for the results shown in Fig. 5b, 5d and 5e, respectively.

All of the time histories (see Fig. 5a,c,e) exhibit some unstructured variation in time, consistent with mild to moderate unsteadiness in general flame structure that was observed in visual imaging of the flames (e.g., see Fig. 3). In the non-aluminized propellant flames, there is a strong correlation between the amplitude of the time variance and the nominal pressure. For example, measurements of temperature exhibited a 1- $\sigma$  precision of 22 K, 50 K, 58 K and 78 K at pressures of 1, 10, 20, and 40 bar, respectively. Similarly, the 1- $\sigma$  precision in  $\chi_{CO}$  was 0.007, 0.013, and 0.021 for pressures of 10, 20, and 40 bar, respectively. When accounting for the time-variation in gas properties (through subtracting the data from a 10-point moving average), the 1- $\sigma$  precision in T at 1, 10, 20 and 40 bar were found to be 0.3%, 0.32%, 0.6%, and 1.1% of the measured value, respectively. Likewise, these values for  $\chi_{CO}$  were, 0.76%, 1.2%, and 3% at 10, 20, and 40 bar, respectively. In the aluminized propellant flames, the temporal variation of gas properties was more pronounced. The 1- $\sigma$  precision in temperature was 88 K and 115 K at 10 and 20 bar, respectively. Similarly, the 1- $\sigma$  precision in  $\chi_{CO}$  was 0.013 and 0.025 at 10 and 20 bar, respectively. Like the non-aluminized cases, these measurements were also obtained with high precision. For temperature, the 1- $\sigma$  precision after accounting for time-variation in gas properties was 0.78% and 1.2% at 10 and 20 bar, respectively. The 1- $\sigma$  precision for  $\chi_{CO}$  was 1.5% and 1.7%. These trends are consistent with the development of increasingly stratified flames as pressure was increased which was observed through visible imaging. In addition, encouragingly, non-absorbing transmission losses

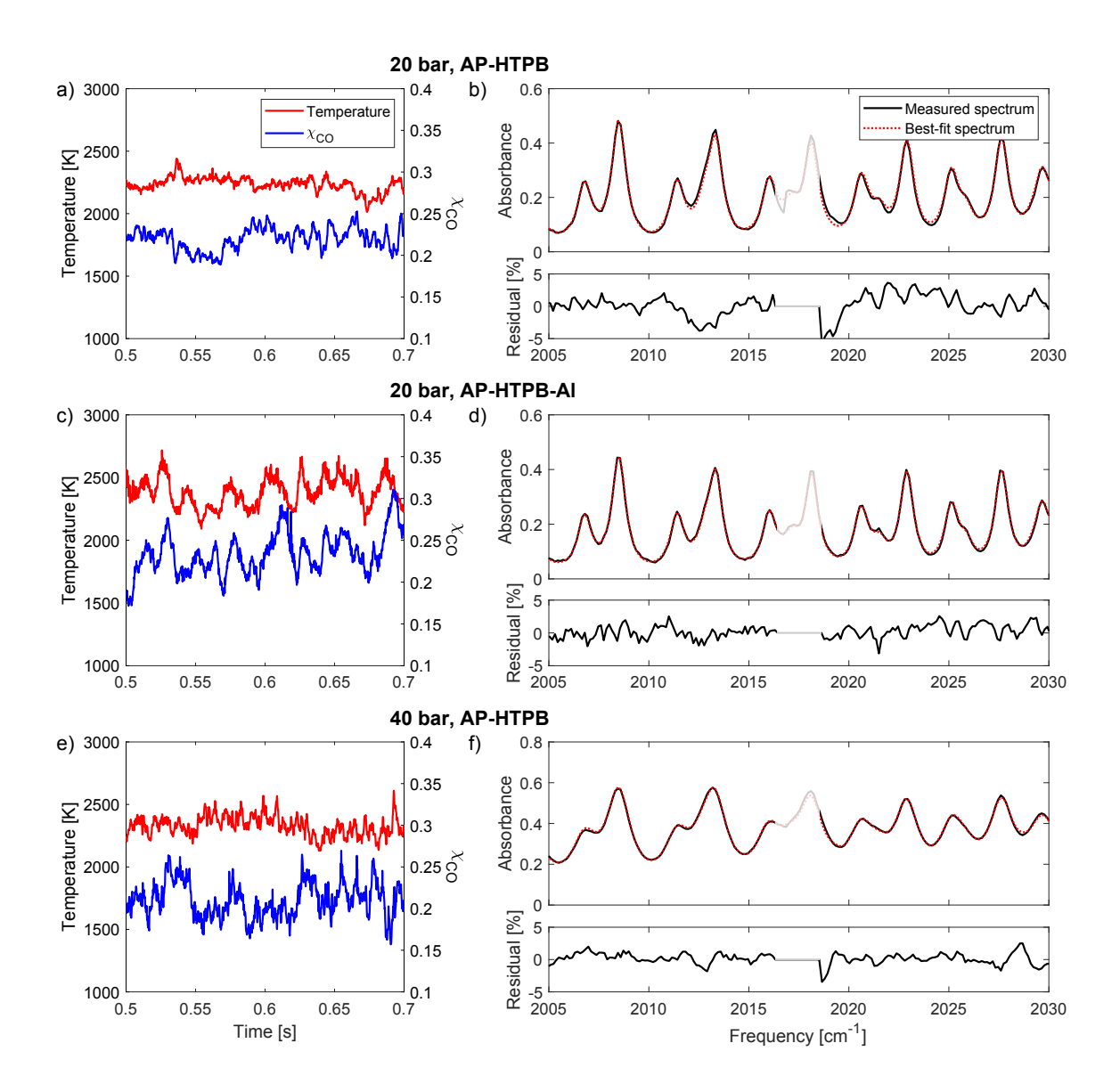


Fig. 5 Samples of measured time histories of temperature and  $\chi_{CO}$  (a, c, e) as well as representative measured and best-fit absorbance spectra of CO with residuals (b, d, f) acquired in propellant tests. Panels a) and b) display results acquired 2 mm above the burning surface of the AP-HTPB propellant at 20 bar. Panels c) and d) display results acquired 1 cm above the burning surface of the Al-AP-HTPB propellant at 20 bar. Panels e) and f) display results acquired 2 mm above the burning surface of the AP-HTPB propellant at 40 bar. The shaded out portion of the spectra was ignored by the spectral-fitting routine due interfering absorption by  $H_2O$  in the ambient air outside the combustion chamber.

did not appear to be exacerbated by the addition of aluminum into the propellant. This suggests that particle scattering and attenuation does not have a significant impact on the transmitted light intensity in these flames.

A notable result is that the time variation in both temperature and  $\chi_{CO}$  increased with pressure as can be seen from inspecting Fig. 5a and 5e. A likely cause for this is the increased burning rate of the propellant at elevated pressures [26, 27] along with the increased gas density which may lead to rapidly changing gas conditions along the measurement

line-of-sight. This is supported by Fig. 3 which shows that as pressure increases, the flames appear more heterogeneous. This effect is exacerbated through the addition of aluminum into the propellant. Product gas plumes of aluminized propellants are inherently heterogeneous environments, with widely varying gas properties due to burning droplets of molten aluminum [28, 29]. As such, these effects are likely responsible for the increased time-variations in T and  $\chi_{CO}$ .

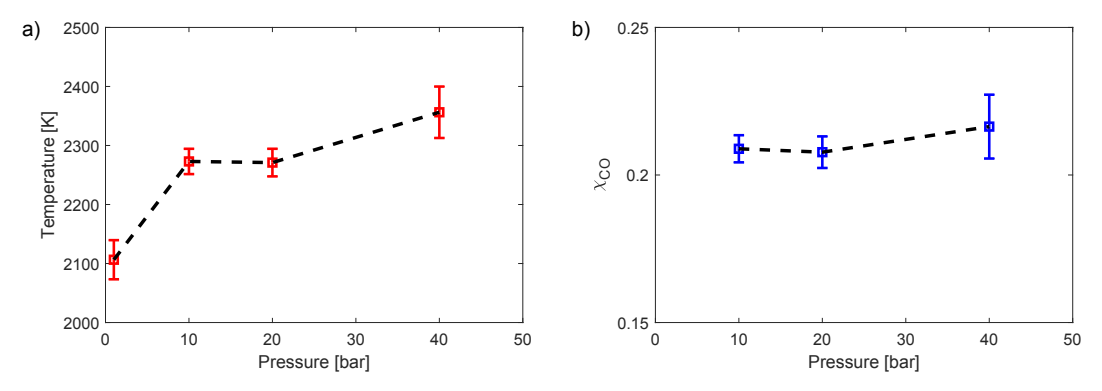


Fig. 6 Time-averaged temperature (a) and  $\chi_{CO}$  (b) measured 2 mm above the propellant surface in AP-HTPB flames. The uncertainty bars represent the 95% confidence interval provided by the nonlinear fitting routine which quantifies the uncertainty induced by measurement noise only.

Figure 6 shows preliminary results for the time-averaged values of temperature and  $\chi_{CO}$  at a measurement location 2 mm above the burning surface of the AP-HTPB propellant at each test condition. These results may change as refinements are made to the spectroscopic model in future work. The measured temperature generally increased with increasing pressure, with the largest temperature rise occurring between 1 and 10 bar which is consistent with predictions from HP equilibrium calculations. In comparison, pressure did not have a detectable impact (i.e., greater than measurement uncertainty) on CO concentration. The average value of  $\chi_{CO}$  was near 0.21 for all cases. This trend in CO concentration with pressure is supported by HP equilibrium calculations.

It is interesting to note that HP equilibrium calculations predict a 50 K increase from 2417 K to 2468 K in the equilibrium flame temperature between 1 and 10 bar, and an approximately 15 K increase between 10 and 40 bar. In contrast, the measurements indicate that the flame temperature increases by a larger amount,  $\approx 175$  K, between 1 and 10 bar. This may result from the fact that at 1 bar the flame gas (originating from AP-HTPB diffusion flames) may not have fully reached equilibrium by 2 mm above the burning surface. Further, it is important to note that the measurements are path-integrated which may partially explain why the measured temperatures at 10 to 40 bar are  $\approx 150$  K below that predicted by HP equilibrium [29]. Incomplete combustion (as evidenced by significant soot production, see Fig. 3) and heat loss to the surrounding bath gas may also partially explain this difference.

# VI. Conclusions

This work presented the first application of ULAS for studying high-pressure combustion gases. ULAS measurements of T and  $\chi_{CO}$  were acquired in AP-HTPB composite-propellant flames at pressures up to 40 bar. Additionally, measurements of T and  $\chi_{CO}$  were acquired in aluminized, AP-HTPB propellant flames, representing some of the first ULAS measurements in multi-phase combustion gases. These propellant flames, both with and without aluminum, represented a challenging test environment for the application of LAS due to the high pressures and long optical path lengths (order of 1 m to spectrometer) required. Ultimately, this led to non-absorbing transmission losses of approximately 90%, however, ULAS was still able to provide high-fidelity measurements due to its broad spectral bandwidth and short (sub-nanosecond) measurement time. The results suggests that the addition of 15% aluminum and, presumably, other metals into the propellant mixture does not significantly effect the performance of the diagnostic, thereby paving the way for future studies of metallized-propellant flames at rocket-motor-relevant pressures.

# Acknowledgments

Funding for this work was provided by AFOSR Grant FA9550-18-1-0210 with Dr. Mitat Birkan as program manager and NSF CBET Award No. 1834972. The authors would like to thank Mingming Gu with assistance and technical

advice regarding the ultrafast laser.

#### References

- [1] Goldenstein, C. S., Spearrin, R. M., Jeffries, J. B., and Hanson, R. K., "Infrared laser-absorption sensing for combustion gases," *Progress in Energy and Combustion Science*, Vol. 60, 2017, pp. 132–176.
- [2] Richardson, D. R., Kearney, S. P., and Guildenbecher, D. R., "Post-detonation fireball thermometry via femtosecond-picosecond coherent anti-Stokes Raman Scattering (CARS)," *Proceedings of the Combustion Institute*, 2020.
- [3] Cole, R. K., Makowiecki, A. S., Hoghooghi, N., and Rieker, G. B., "Baseline-free quantitative absorption spectroscopy based on cepstral analysis," *Optics Express*, Vol. 27, No. 26, 2019, pp. 37920–37939.
- [4] Goldenstein, C. S., Mathews, G. C., Cole, R. K., Makowiecki, A. S., and Rieker, G. B., "Cepstral Analysis for Baseline-Insensitive Absorption Spectroscopy Using Light Sources with Pronounced Intensity Variations," *Applied Optics*, Vol. 59, No. 26, 2020, pp. 7865–7875.
- [5] Bendana, F. A., Lee, D. D., Schumaker, S. A., Danczyk, S. A., and Spearrin, R. M., "Cross-band infrared laser absorption of carbon monoxide for thermometry and species sensing in high-pressure rocket flows," *Applied Physics B*, Vol. 125, No. 11, 2019, p. 204.
- [6] Tancin, R. J., Mathews, G. C., and Goldenstein, C. S., "Design and application of a high-pressure combustion chamber for studying propellant flames with laser diagnostics," *Review of Scientific Instruments*, Vol. 90, No. 4, 2019, p. 045111.
- [7] Goldenstein, C. S., Spearrin, R. M., Jeffries, J. B., and Hanson, R. K., "Infrared laser absorption sensors for multiple performance parameters in a detonation combustor," *Proceedings of the Combustion Institute*, Vol. 35, No. 3, 2015, pp. 3739–3747.
- [8] Goldenstein, C. S., Almodóvar, C. A., Jeffries, J. B., Hanson, R. K., and Brophy, C. M., "High-bandwidth scanned-wavelength-modulation spectroscopy sensors for temperature and H<sub>2</sub>O in a rotating detonation engine," *Measurement Science and Technology*, Vol. 25, No. 10, 2014, p. 105104.
- [9] Tancin, R. J., Chang, Z., Gu, M., Radhakrishna, V., Lucht, R. P., and Goldenstein, C. S., "Ultrafast laser-absorption spectroscopy for single-shot, mid-infrared measurements of temperature, CO, and CH<sub>4</sub> in flames," *Optics Letters*, Vol. 45, No. 2, 2020, pp. 583–586.
- [10] Caswell, A. W., Roy, S., An, X., Sanders, S. T., Schauer, F. R., and Gord, J. R., "Measurements of multiple gas parameters in a pulsed-detonation combustor using time-division-multiplexed Fourier-domain mode-locked lasers," *Applied Optics*, Vol. 52, No. 12, 2013, pp. 2893–2904.
- [11] Schlosser, E., Fernholz, T., Teichert, H., and Ebert, V., "In situ detection of potassium atoms in high-temperature coal-combustion systems using near-infrared-diode lasers," *Spectrochimica Acta Part A: Molecular and Biomolecular Spectroscopy*, Vol. 58, No. 11, 2002, pp. 2347–2359.
- [12] Draper, A. D., Cole, R. K., Makowiecki, A. S., Mohr, J., Zdanowicz, A., Marchese, A., Hoghooghi, N., and Rieker, G. B., "Broadband dual-frequency comb spectroscopy in a rapid compression machine," *Optics Express*, Vol. 27, No. 8, 2019, pp. 10814–10825.
- [13] Nair, A. P., Lee, D. D., Pineda, D. I., Kriesel, J., Hargus, W. A., Bennewitz, J. W., Danczyk, S. A., and Spearrin, R. M., "MHz laser absorption spectroscopy via diplexed RF modulation for pressure, temperature, and species in rotating detonation rocket flows," *Applied Physics B*, Vol. 126, No. 8, 2020, pp. 126–138.
- [14] Rein, K. D., Roy, S., Sanders, S. T., Caswell, A. W., Schauer, F. R., and Gord, J. R., "Measurements of gas temperatures at 100 kHz within the annulus of a rotating detonation engine," *Applied Physics B*, Vol. 123, No. 3, 2017, p. 88.
- [15] Sanders, S. T., Mattison, D. W., Ma, L., Jeffries, J. B., and Hanson, R. K., "Wavelength-agile diode-laser sensing strategies for monitoring gas properties in optically harsh flows: application in cesium-seeded pulse detonation engine," *Optics Express*, Vol. 10, No. 12, 2002, pp. 505–514.
- [16] Mathews, G. C., Blaisdell, M. G., Lemcherfi, C. D., Aaron I. Slabaugh, and Goldenstein, C. S., "High-Bandwidth Laser-Absorption Measurements of Temperature, Pressure, CO, and H<sub>2</sub>O in the Annulus of a Rotating Detonation Rocket Engine," 2021, p. 1.
- [17] Mathews, G. C., and Goldenstein, C. S., "Near-GHz scanned-wavelength-modulation spectroscopy for MHz thermometry and H<sub>2</sub>O measurements in aluminized fireballs of energetic materials," *Applied Physics B*, Vol. 126, No. 11, 2020, pp. 1–17.

- [18] Tancin, R. J., Chang, Z., Radhakrishna, V., Gu, M., Lucht, R. P., and Goldenstein, C. S., "Ultrafast Laser Absorption Spectroscopy in the Mid-Infrared for Measuring Temperature and Species in Combustion Gases," AIAA Scitech 2020 Forum, 2020, p. 0517.
- [19] Radhakrishna, V., Tancin, R. J., Mathews, G. C., Lucht, R. P., and Goldenstein, C. S., "Single-shot ultrafast-laser-absorption measurements of temperature, CO, NO, and H<sub>2</sub>O in HMX fireballs," AIAA Scitech 2021 Forum, 2021, p. 1.
- [20] Lee, D. D., Bendana, F. A., Schumaker, S. A., and Spearrin, R. M., "Wavelength modulation spectroscopy near 5 μm for carbon monoxide sensing in a high-pressure kerosene-fueled liquid rocket combustor," Applied Physics B, Vol. 124, No. 5, 2018, p. 77.
- [21] Schwarm, K. K., Dinh, H. Q., Goldenstein, C. S., Pineda, D. I., and Spearrin, R. M., "High-pressure and high-temperature gas cell for absorption spectroscopy studies at wavelengths up to 8 μm," *Journal of Quantitative Spectroscopy and Radiative Transfer*, Vol. 227, 2019, pp. 145–151.
- [22] Goldenstein, C. S., Miller, V. A., Spearrin, R. M., and Strand, C. L., "SpectraPlot. com: Integrated spectroscopic modeling of atomic and molecular gases," *Journal of Quantitative Spectroscopy and Radiative Transfer*, Vol. 200, 2017, pp. 249–257.
- [23] Hargreaves, R., Gordon, I., Kochanov, R., and Rothman, L., "HITEMP: Extensive molecular line lists for high-temperature exoplanet atmospheres," EPSC, Vol. 2019, 2019, pp. EPSC–DPS2019.
- [24] Rothman, L., Gordon, I., Barber, R., Dothe, H., Gamache, R., Goldman, A., Perevalov, V., Tashkun, S., and Tennyson, J., "HITEMP, the high-temperature molecular spectroscopic database," *Journal of Quantitative Spectroscopy and Radiative Transfer*, Vol. 111, No. 15, 2010, pp. 2139–2150.
- [25] Hartmann, J.-M., Rosenmann, L., Perrin, M.-Y., and Taine, J., "Accurate calculated tabulations of CO line broadening by H<sub>2</sub>O, N<sub>2</sub>, O<sub>2</sub>, and CO<sub>2</sub> in the 200-3000 K temperature range," *Applied Optics*, Vol. 27, No. 15, 1988, pp. 3063–3065.
- [26] Dennis, C., and Bojko, B., "On the combustion of heterogeneous AP/HTPB composite propellants: A review," Fuel, Vol. 254, 2019, p. 115646.
- [27] Cai, W., Thakre, P., and Yang, V., "A model of AP/HTPB composite propellant combustion in rocket-motor environments," *Combustion Science and Technology*, Vol. 180, No. 12, 2008, pp. 2143–2169.
- [28] Kearney, S. P., and Guildenbecher, D. R., "Temperature measurements in metalized propellant combustion using hybrid fs/ps coherent anti-Stokes Raman scattering," *Applied Optics*, Vol. 55, No. 18, 2016, pp. 4958–4966.
- [29] Ruesch, M. D., McDonald, A. J., Mathews, G. C., Son, S. F., and Goldenstein, C. S., "Characterization of the influence of aluminum particle size on the temperature of composite-propellant flames using CO absorption and AlO emission spectroscopy," *Proceedings of the Combustion Institute*, 2020.